Lab on a Chip

RSC Publishing

PAPER

View Article Online
View Journal | View Issue

Cite this: *Lab Chip*, 2013, **13**, 1357

Needle-free injection into skin and soft matter with highly focused microjets

Yoshiyuki Tagawa,†*[a] Nikolai Oudalov,[a] A. El Ghalbzouri,[b] Chao Sun*[a] and Detlef Lohse*[a]

Received 30th October 2012,
Accepted 3rd January 2013

DOI: 10.1039/c2lc41204g

www.rsc.org/loc

The development of needle-free drug injection systems is of great importance to global healthcare. However, in spite of its great potential and research history over many decades, these systems are not commonly used. One of the main problems is that existing methods use diffusive jets, which result in scattered penetration and severe deceleration of the jets, causing frequent pain and insufficient penetration. Another long-standing challenge is the development of accurate small volume injections. In this paper we employ a novel method of needle-free drug injection, using highly-focused high speed microjets, which aims to solve these challenges. We experimentally demonstrate that these unique jets are able to penetrate human skin: the focused nature of these microjets creates an injection spot smaller than a mosquito's proboscis and guarantees a high percentage of the liquid being injected. The liquid substances can be delivered to a much larger depth than conventional methods, and create a well-controlled dispersion pattern. Thanks to the excellent controllability of the microjet, small volume injections become feasible. Furthermore, the penetration dynamics is studied through experiments performed on gelatin mixtures (human soft tissue equivalent) and human skin, agreeing well with a viscous stress model which we develop. This model predicts the depth of the penetration into both human skin and soft tissue. The results presented here take needle-free injections a step closer to widespread use.

1 Introduction

The development of needle-free drug injection systems is an essential part of the global fight against the spread of disease.[1–3] Contamination, needle-stick injuries,[4] painful injections, and needle phobia[5] are issues related to traditional syringe injections with needles that demand attention. Needle-free injections systems offer the prospect of resolving these problems.[6] Previous studies have explored the possibilities of needle-free injections, but important limitations still need to be addressed.[7–12]

The main issue that is limiting applicability is the shape of the jets produced by the current systems. These devices create diffusive jets, leading to a large dispersion pattern and unreliable penetration. This in turn can create problems for patients, in the form of frequent bruising and pain.[12] The small nozzle can easily get clogged, causing disruptions to controllability. It is difficult to avoid diffusive shape of microjets for methods which essentially consists of a syringe filled with drug and a piston. Taberner and co-workers[13–15] developed a device comprising of a syringe with a Lorenz-force motor to tackle these problems. This device can monitor the speed of the jet and regulate the volume of drug.

Very recently, we have managed to generate thin, focused microjets with velocities of up to 850 m s^{-1} by the rapid vaporization of a small mass of liquid in an open liquid-filled capillary.[16] In terms of its application to needle-free injection devices, the main advantage of our method in contrast with other methods is the highly focused shape of microjets with sufficiently high velocities. The width of the hole inside the soft material created by this jet keeps as tiny as the jet diameter $\sim$30 μm. This can suppress severe pain for patients. Ultra-high velocities (more than 200 m s^{-1}) enable one-shot penetration to the desired area and good controllability.

Due to the fine scale of the jet tip (30 μm) combined with the high velocities, we can easily adjust the penetration depth according to the requirements. This makes drug delivery efficient and as painless as possible.

In this article we study the penetration dynamics of these highly focused microjets into gelatin mixtures and artificially grown human skin using high-speed imaging. We investigate the penetration depth as a function of the jet velocity and the capillary tube diameter. The understanding of these dynamics

[a]*Physics of Fluids Group, MESA+ Institute and Faculty of Science and Technology, Burgers Centre for Fluid Dynamics, University of Twente, P.O. Box 217, 7500 AE Enschede, Netherlands. E-mail: y.tagawa@utwente.nl; c.sun@utwente.nl; d.lohse@utwente.nl; Fax: + 31 53 489 8068; Tel: + 31 53 489 2470*
[b]*Department of Dermatology, Leiden University Medical Center, Leiden, The Netherlands*
† Current address: Department of Mechanical Systems Engineering, Tokyo University of Agriculture and Technology, Tokyo, Japan. E-mail: tagawayo@cc.tuat.ac.jp

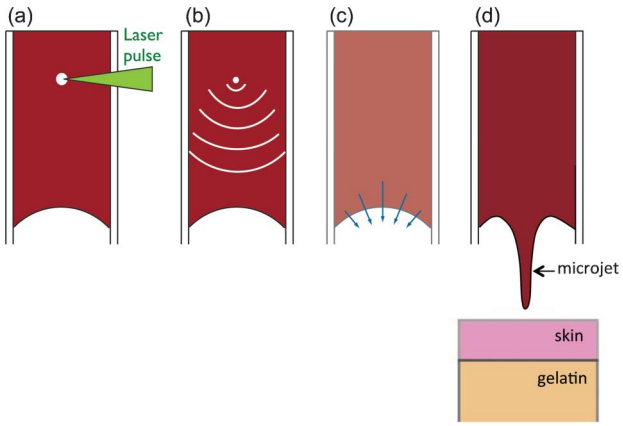

Fig. 1 Schematic illustration for the microjet generation and the testing system. (a) A vapor bubble is created immediately after the illumination of a focused laser pulse into a capillary tube filled with water-based red dye. (b) The abrupt expansion of this vapor bubble leads to a shock wave propagating towards the liquid interface. (c) Due to the curved interface, kinematic focusing occurs and causes a highly-focused high-speed microjet. (d) The microjet impacts the reference material, comprising of pure gelatin 5 wt% or skin layer (LKE) on top of the gelatin.

will provide essential insight for the development of needle-free injection devices.

2 Material and methods

2.1 Microjet generation

Fig. 1 shows a sketch of microjet generation and testing system. The microjet generation system is the same as that used by Tagawa *et al.*:[16] We focus a laser pulse (100 mJ Nd:YAG laser, 532 nm, 6 ns pulse, Solo PIV, New Wave Research, USA) through a 10 × objective to small volume in a capillary tube, which is filled with water-based red dye. The range of the power for the laser in the tests is 0–20 mJ. This leads to the abrupt vaporization of a small mass of liquid[23] (see Fig. 1a). The vaporization causes a shock wave to travel through the liquid (Fig. 1b) and impulsively accelerate the curved liquid interface due to kinematic focusing (Fig. 1c). The microjet impacts the reference material which resembles real human body as described below. The capillary tube is connected to a syringe through micro tubing and the working fluid (dye) is pumped into the capillary tube using a syringe pump (Model PHD 2000, Harvard Apparatus, USA). The characteristics of this jet, such as velocity and width, can be controlled by varying the laser power, the distance between the laser focus and the free surface, the liquid-glass contact angle, and the diameter of the tube.[16] With given parameters in this study, the jet velocity μ (m s^{-1}) linearly increases with the laser energy E (J) absorbed in the liquid.[16] For a nozzle of 500 μm in diameter, we have

$$u = 1.2 \times 10^5 E - 24.13. \quad (1)$$

Note that the forces exerted on the liquid that is delivered with ultra-high velocities cause minor damage to the medicine that is contained in it.[17] The vaporization of the liquid through the use of the laser could damage the drug molecules. However, the volume of the focused laser spot in this study is in the order of 10^{-15} L, which is small compared to that of microjet in the order of 10^{-9} L. Moreover, the distance from the meniscus and the laser spot is ~0.6 mm, which is about 60 times larger than the size of the laser spot. We hence assume that the microjet emerging from the liquid very close to the interface is not affected by this method.

2.2 Injection into gelatin

Gelatin mixtures were used to study the injection into solid substrates. The gelatin was prepared a few hours before the experiments by dissolving 5 weight% of gelatin in MilliQ water. After dissolving the gelatin, the mixture was poured into small 1 cm × 1 cm cuvettes and put in the fridge (4 °C) for an hour. Penetration dynamics were filmed using high-speed cameras with frame rates up to 10^6 fps (HPV-1, Shimadzu Corporation, Japan, and FASTCAM SAX, Photron, USA).

2.3 Penetration across human skin *in vitro*

The artificial skin was cultured by the Department of Dermatology of the Leiden University Medical Center. The Leiden human Epidermal skin Model (LEM) used in this study has been fully characterized and shows very high similarities with native skin.[26] The LEM represents a full-thickness model (epidermis generated onto a dermal matrix). The competency of the skin barrier depends mainly on the lipid composition and organization. From a mechanical point of view, stratum corneum (SC) plays a dominant role due to its high mechanical strength. The SC of LEM contains all barrier lipid classes that are present in native human skin: The three lipid classes present in human SC, namely cholesterol, free fatty acids and ceramides, are also present in the SC of the LEM. In addition, the LEM show the presence of all ceramide subclasses that are present in native human SC.[24] By using a safranin red staining, we have shown that our in-house skin models have similar SC thickness as native skin, 11.3 ± 1.5 and 11.4 ± 1.2 SC layers, respectively.[25] Concerning the epidermis, the LEMs used in this study have similar epidermal thickness compared to native skin (± 80–100 μm). The penetration of several chemicals and the ET50 assay using Triton-X 100 demonstrates that the barrier properties are comparable as native skin.[26] The skin was supplied in patches of 2.4 cm in diameter and was kept in an incubator prior to experiments. For the penetration experiments, the skin layers were placed on top of the gelatin mixtures in the small cuvettes. Penetration dynamics were filmed using high-speed cameras (HPV-1, Shimadzu Corporation, Japan, and FASTCAM SAX, Photron, USA).

2.4 Velocity and depth measurement

High-speed cameras (HPV-1, Shimadzu Corporation, Japan, and FASTCAM SAX, Photron, USA) were used to record the injection process. The velocity and depth were determined from these high-speed recordings.

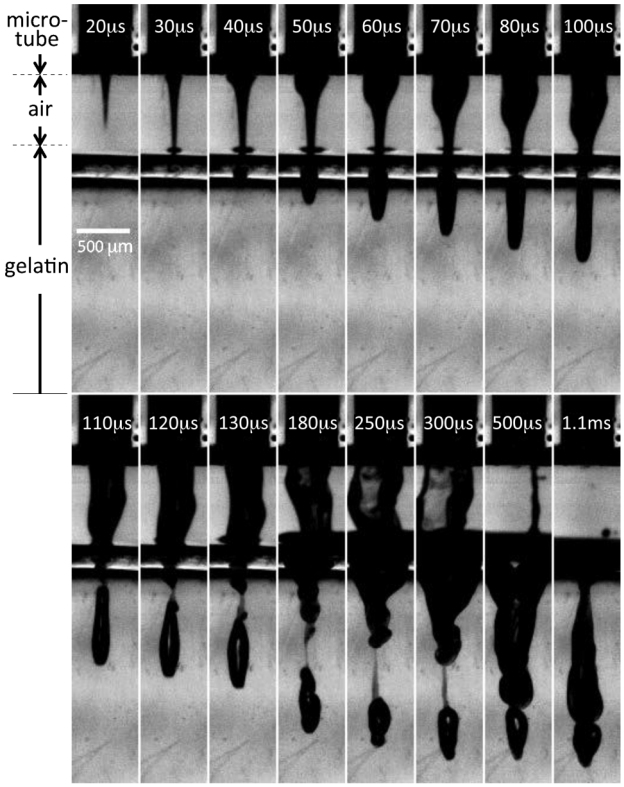

Fig. 2 Snapshots of the jet penetration into gelatin. The laser is shot at 0 μs and the subsequent images show the jet injection process at the designated times. The jet is created in a 500 μm tube.

3 Results and discussion

3.1 Injection into gelatin

In order to study the penetration of these microjets, we used gelatin 5 wt% as a model material. This percentage simulates the properties of soft tissue in the human body.[8] Fig. 2 provides the first observation of the temporal evolution of the jet penetration. This visualization is of utmost importance for studying the interaction of the microjet and the human body. As illustrated in Fig. 2, the sharp tip of the microjet reaches the material first. The diameter of this tip creates an injection spot ~30 μm, smaller than a mosquito's proboscis. This thin part of the jet starts digging a hole into the material. Thanks to the highly focused geometry, there is no splashing around the penetration spot, which is crucial for medical applications. This is clearly indicated in Fig. 2 for the snapshots covering 30–100 μs. The snapshot at 100 μs shows a well-controlled dispersion pattern. The width of the hole remains as small as the jet diameter. This is in sharp contrast to the existing methods using diffusive jets, which result in scattered penetration. The low-speed thick part of the jet utilizes the entry point created by the thin jet and is efficiently deposited into the material. The penetration of the tip stops at about 300 μs while the thick jet part continues to make its way to the deepest part of the hole. At the final snapshot (1.1 ms) the most of the liquid has passed through the skin (~10 nL) and there is a very small drop (~1 nL) remaining outside. Thus the

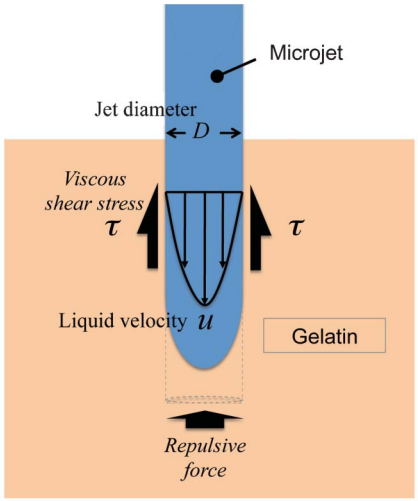

Fig. 3 The schematic sketch of the forces acting on the jet. The jet shown by the blue color region is penetrating into the gelatin. The viscous shear stress τ acts at the interface between liquid and gelatin due to the shear flow inside the jet. The repulsive force acts vertically on the projection area of the jet shown by the dashed closed line.

efficiency of delivering the liquid into the skin in this case is ~90%, *i.e.* a high percentage of the liquid in the microjet penetrates into the skin model. The entire process is finished after 1.1 ms.

Fig. 4 shows the penetration depth of the microjet generated in a 200 μm tube into gelatin 5 wt% as a function of the jet velocity. Each datapoint in Fig. 3 represents a single penetration event of the jet into the gelatin. The depth linearly increases with the jet velocity, covering depths from several

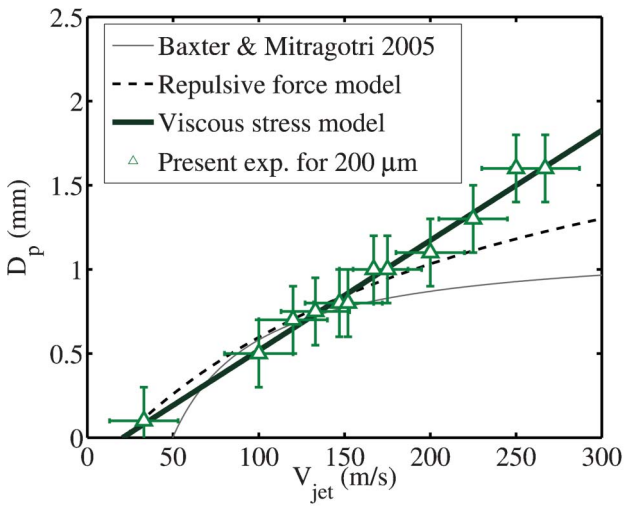

Fig. 4 Injection depth as a function of the jet velocity. Green triangles show the experimental results for the 200 μm tube. The depth increases with the jet velocity and no saturation tendency is observed. For comparison, the gray thin line shows the Baxter model, the blue dashed line is the repulsive force model, and the black thick line is the viscous stress model with same offset. The experimental results agree well with this latter model.

hundred microns at low jet speed to ~1.5 millimeter when the jet velocity approaches ~250 m s^{-1}. This highlights the versatility of this method, making it adjustable to different skin-properties (*e.g.* children/adults, different skin types) and to a broad range of medical applications (*e.g.* insulin injection,[18,19] vaccinations,[20–22] or medical tattoos).

To get a quantitative understanding, we compare the present results with various models. A model proposed by Baxter *et al.*[10] is fitted to this experimental data and presented in the figure. The agreement in the low velocity region is fair. However, this model shows a saturation of the penetration depth for velocities above 200 m s^{-1}. In our experiments we did not observe this trend as can be seen in Fig. 4. The difference is likely due to the shape of the jet created using our novel method. The jet shape created by conventional methods using syringe-piston system (*e.g.*[7,8,10]) is diffusive. This shape leads to severe deceleration with jet travel distance (especially for high velocities), which is considered in the model by Baxter *et al.*,[10] resulting in shallow penetration. On the other hand, the highly focused jets in our experiments do not experience this significant deceleration.

To address this discrepancy we consider the relation between initial impact velocity of the jet and the drag force. We observe that the gelatin does not show much deformation and the jet penetrates into gelatin with cylindrical shape (see the snapshots at 100 μs in Fig. 2). We model this phenomena as a cylindrical microjet, normal to the gelatin surface. It creates a cylindrical 'crack' inside the gelatin, which keeps the same circular projection area independent of the depth. Fig. 3 shows the schematic sketch of this model. The drag forces on the jet are the viscous shear stress at the jet-gelatin interface and the repulsive force on the area of the cross-section of the jet. We consider two basic force models, representing these two different cases: A viscous stress model and a repulsive force model.

We first introduce the viscous stress model. The viscous shear stress τ_w at the wall is $\mu\partial u/\partial r$, where μ is the dynamic viscosity of the liquid, μ is the liquid velocity component in the direction parallel to the wall, and r is the normal position to the wall. In the present case, the velocity scale and the length scale for τ_w are v and D, respectively. In the viscous regime the relationship between the velocity and the drag force per unit mass is:

$$F_D = -c_v\, v, \tag{2}$$

where c_v is a fitting parameter with the units of inverse time. It is known that gentle deposition (small impact velocity) into the soft matter gives no penetration. The penetration starts when the impact velocity v_{jet} exceeds a critical velocity v_c. For $v_{jet} \geqslant v_c$ the final penetration depth D_p is given by:

$$D_p = \frac{1}{c_v}(v_{jet} - v_c). \tag{3}$$

The other model considers a repulsive force acting on the jet. The repulsive force is modeled as being proportional to the inertial force of the jet ($\sim \rho v^2$). In this inertial regime, the relationship between the velocity and the drag force per unit mass is given by:

$$F_D = -c_i\, v^2, \tag{4}$$

where c_i is a fitting parameter with dimensions of inverse length. Including the offset due to the critical velocity, we obtain the final penetration depth D_p as:

$$D_p = \frac{1}{c_i}\ln\left(\frac{v_{jet}}{v_c} - 1\right). \tag{5}$$

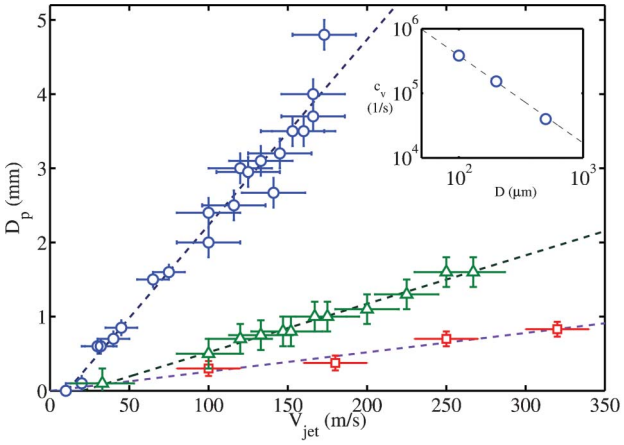

Fig. 5 Injection depth as a function of the jet velocity for different capillary tube diameters. The data for each capillary tube are fitted by the viscous stress model, shown by the dashed line. The fitted slope c_v is plotted as a function of the capillary size in the inset. The data can be represented by $c_v \propto D^{-1.35\ \pm\ 0.48}$, shown as the black dash-dotted line in the inset.

Both models are compared with the experimental results in Fig. 4. It shows that the viscous stress model gives the best agreement, indicating that the jet likely experiences shear stress in the material. This model gives predictive power to our novel method, enabling us to link the physical parameters of our lab experiments to real world medical applications.

Fig. 5 shows the penetration depth for the jets created in tubes with three different diameters. As discussed by Tagawa *et al.*,[16] tubes with larger diameters result in jets with larger diameters. At the same time, the penetration depth increases with the diameter of the jet. For the 500 μm tube case, the jet can penetrate up to ~5 mm in a single shot. For the 100 μm tube case, the jet penetrates 0.5 mm at a velocity of 320 m s^{-1}, close to sonic speed. Thanks to the large velocity range of our jets, we can achieve the same penetration depth by using different tube diameters, which enables us to control the injection volume with nano-liter precision.

All data sets show a linear relation between the penetration depth and the jet velocity. Remarkably the viscous stress model eqn (3) discussed above holds for all cases. We will now try to calculate the parameter c_v in eqn (3) from the jet geometry: We approximate the jet shape by a cylinder, whose mass $m_j = \pi\rho D^2 l/4$, where l is the length of the jet cylinder. The total viscous stress on the jet is $F_v = \int_{dA} \tau dA$, where A is the area

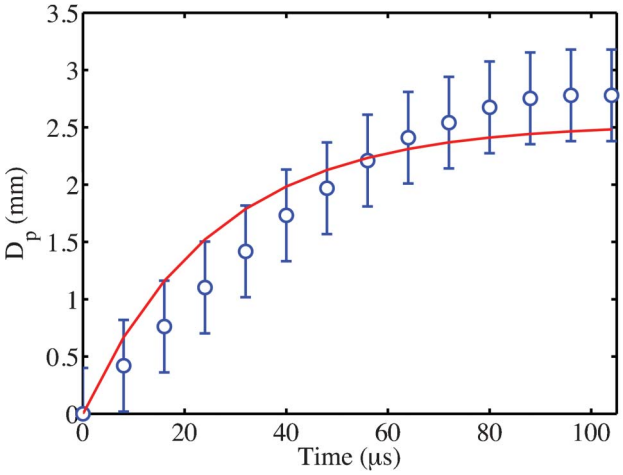

Fig. 6 The time evolution of the penetration depth D_p. The blue markers show the experimental results for the jet of v_{jet} = 120 m s^{-1} for the 500 μm tube. The red thick line shows the penetration depth from eqn (6) with c_v obtained by fitting the model by eqn (3) to all data for the 500 μm tube shown in Fig. 5.

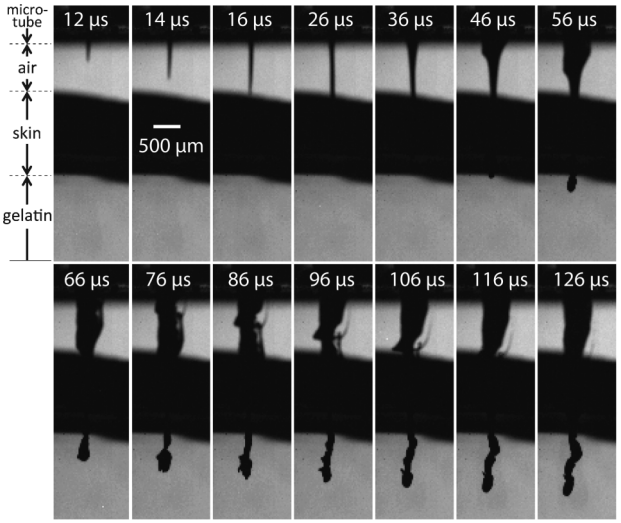

Fig. 7 Time evolution of the jet penetration into human skin placed on gelatin. After the second snapshot, the time interval for each image is 10 μs. The laser is shot at 0 μs. The jet impact velocity is 160 m s^{-1}. Note that the dark region of the skin in the images is thicker than the actual thickness of the skin, as the skin curls up on the sides of the cuvette.

on which the viscous shear stress acts. The elongated shape of the jet, *i.e.* the aspect ratio $D/l \ll 1$ allows us to approximate $A \approx \pi Dl$, leading to $F_v \sim \mu v l$. Thus we obtain eqn (2) $F_D \sim c_v v$ with $c_v \propto D^{-2}$, meaning that c_v quadratically decreases with increasing D. The experimental values c_v for each tube jet are shown in the inset in the Fig. 5. Indeed, larger values for c_v are found for smaller D. Assuming a power low $c_v \propto D^{\alpha}$ we obtain from the experimental results $\alpha = -1.35 \pm 0.48$, slightly larger than the model result $\alpha = -2$.

We also experimentally measure the time evolution of the penetration depth and compare it with the viscous stress model. The model leads to an exponential temporal evolution of the penetration depth $D_p(t)$,

$$D_p(t) = \frac{v_{jet} - v_c}{c_v}(1 - e^{-c_v t}). \quad (6)$$

The viscous stress model shows an agreement with the measurement within error bars as shown in Fig. 6. This result provides additional support in favor of the viscous stress model for gelatin.

3.2 Injection into artificially grown human skin

In order to mimic the real human body, we have used artificially grown human skin placed on top of the gelatin 5 wt% as a target material for our jets. Fig. 7 shows snapshots of the jet penetrating into this material comprising of both the skin and the gelatin. The tip of the jet is observed for the first time in the gelatin at 46 μs. At this point, it is clear that the jet is able to penetrate human skin. After this stage, the penetration dynamics are similar to those in the gelatin case shown in Fig. 2. We visually observed that the volume of penetrated liquid is very much comparable to Fig. 2. The jet is still focused even though the jet has to penetrate through the additional barrier of skin.

Fig. 8(b) shows the penetration depth (D_p) into the gelatin through the skin as a function of the initial impact velocity (V_{jet}) of the jet. Note that the data only represent the penetration depth (D_p) into the gelatin, excluding the skin thickness (l_s) as indicated in Fig. 8(a). The threshold velocity for penetrating through the skin is found to be 80 m s^{-1}. Even after the jet has penetrated an additional barrier in the form of human skin, the depth depends linearly on the initial velocity (V_{jet}). This suggests an excellent controllability of this system, which is crucial for medical applications. As seen in Fig. 8(b), the jet can penetrate more than a millimeter into the soft tissues (gelatin in the present case), after passing through the skin barrier. This depth is sufficient for most medical applications, *e.g.* insulin injection or vaccinations. When compared to the pure gelatin case (dashed line in Fig. 8(b)), the penetration depth is of course smaller with the skin layer being present. The skin decelerates the jet until complete penetration through itself (at $t = t_1$ as shown in Fig. 8(a)), after which the jet penetrates the gelatin until complete stoppage (at $t = t_2$). For the latter process we again adopt the viscous drag model, but with a reduced velocity v_{sg} due to the additional barrier of the skin (as shown in Fig. 8(a)). The velocity reduction by the skin layer is

$$\Delta V = V_{jet} - V_{sg}, \quad (7)$$

which, as indicated in Fig. 8(b), is equivalent to the horizontal offset between the line for the pure gelatin and the measured data with the skin layer being present. Fig. 8(c) shows this velocity reduction (ΔV) as a function of the impact velocity (V_{jet}).

We evaluate the velocity reduction by considering the drag of the skin layer again with two different models: the viscous stress model and the repulsive force model. The viscous stress

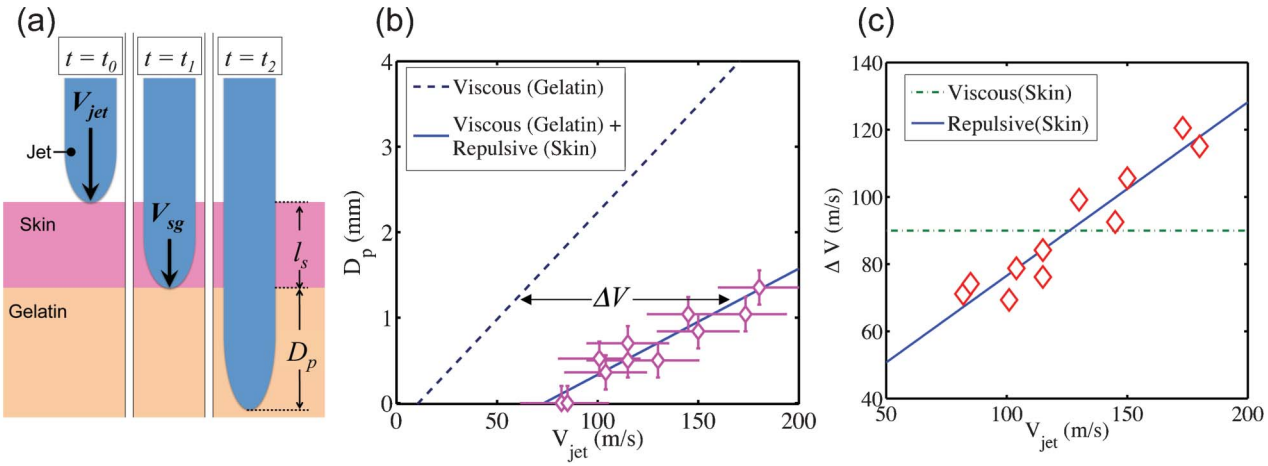

Fig. 8 (a) A sketch for the jet penetration into the gelatin covered with the artificially grown human skin layer (the thickness l_s = 700 μm). At $t = t_0$ the jet impacts the skin layer with the velocity V_{jet}. At $t = t_1$ the jet goes through the skin layer and start penetrating the gelatin with the velocity V_{sg}. At $t = t_2$ the jet stops at the final depth D_p. (b) Diamonds: the final depth D_p into gelatin with the skin layer as a function of the jet velocity. The dashed line: the case for gelatin without skin attached. The blue thick line: the results of the model represented by eqn (9). (c) The velocity reduction ΔV due to the skin layer *vs.* the impact velocity. The dark green line: the viscous stress model for the skin, and the blue thick line: the repulsive force model eqn (8).

model for the skin layer leads to a constant velocity reduction for a given skin thickness (see eqn (3)). However, the experimental results show a different trend in Fig. 8(c). Hence, we model the skin layer with a repulsive force (see eqn (4)), and the corresponding velocity reduction is

$$\Delta V = v_{jet} - (v_{jet} - v_s)e^{-c_{i,s}l_s}, \quad (8)$$

with two fitting parameters: $c_{i,s}$ and v_s, and the skin thickness l_s = 700 μm. Fig. 8(c) reveals that the model described by eqn (8) with $c_{i,s} = 1.0 \times 10^3$ m^{-1} and $v_s = 51.5$ m s^{-1} shows a good agreement with the experiments, suggesting that the jet experiences the repulsive force in the skin layer. This is probably due to the increased hardness of the skin compared to that of gelatin. The final penetration depth inside the gelatin can be therefore obtained as

$$D_p = \frac{1}{c_v}((v_{jet} - v_s)e^{-c_{i,s}l_s} - v_c), \quad (9)$$

which is plotted as the thick line in Fig. 8(b). The excellent agreement suggests that the model eqn (9) combining the repulsive force for the skin layer and the viscous drag for the gelatin, nicely describes the depth of the jet penetration. This model is thus suited to quantitatively describe the penetration of high-speed jets into human skin enclosing soft tissue and thus this result takes needle-free injections a step closer to widespread use. Furthermore if a *portable* pulse-laser device is invented, one could use it to develop convenient-to-use handheld needle-free injection devices.

4 Conclusions

In this study we have shown that a novel method for needle-free injections can resolve many of the long-standing issues that have prevented large-scale adaptation of needle-free injection systems. We show that a highly-focused geometry of the jets and a wide range of velocities is essential for good controllability, versatility, and effectiveness of needle-free injection systems. We also model the penetration of the jet into soft matter and human skin enclosing soft tissue. The results presented here take needle-free injections a step closer to widespread use.

Acknowledgements

We thank C. Clanet, F. Dijksman, B. Hoeksma, L. Homan, Devaraj van der Meer, Vivek N. Prakash, and C.W. Visser for fruitful discussions. We appreciate the financial support given by Fundamenteel Onderzoek der Materie (FOM), which is part of Nederlandse Organisatie voor Wetenschappelijk Onderzoek (NWO) and the European Research Council (ERC) through a Proof of Concept Grant.

References

1 A. Kane, J. Lloyd, M. Zaffran, L. Simonsen and M. Kane, *Bull. World Health Organ.*, 1999, **77**, 801–807.
2 H. Varmus, R. Klausner, E. Zerhouni, T. Acharya, A. S. Daar and P. A. Singer, *Science*, 2003, **17**, 398–399.
3 A. M. Hauri, G. L. Armstrong and Y. J. F. Hutin, *Int. J. STD AIDS*, 2004, **15**, 7–16.
4 M. Kermode, *Health Promot. Int.*, 2004, **19**, 95–103.
5 Y. Nir, A. Paz, E. Sabo and I. Potsman, *Am. J. Trop. Med. Hyg.*, 2003, **68**, 341–344.
6 S. Mitragotri, *Nature Rev. Immunol.*, 2005, **5**, 905–916.
7 A. Arora, I. Hakim, J. Baxter, R. Rathnasingham, R. Srinivasan, D. A. Fletcher and S. Mitragotri, *Proc. Nat. Acad. Sci.*, 2007, **104**, 4255–4260.

8 V. Menezes, S. Kumar and K. Takayama, *J. Appl. Phys.*, 2009, **106**, 086102.
9 J. C. Stachowiak, T. H. Li, A. Arora, S. Mitragotri and D. A. Fletcher, *J. Controlled Release*, 2009, **135**, 104–112.
10 J. Baxter and S. Mitragotri, *J. Controlled Release*, 2005, **106**, 361–373.
11 J. Schramm-Baxter and S. Mitragotri, *J. Controlled Release*, 2004, **97**, 527–535.
12 S. Mitragotri, *Nature Rev. Drug Discovery*, 2006, **5**, 543–548.
13 A. Taberner, N. C. Hogan and I. W. Hunter, *Medical Eng.*, 2012, **34**, 1228–1235.
14 B. D. Hemond, A. Taberner, N. C. Hogan, B. Crane and I. W. Hunter, *J. Med. Devices*, 2011, **5**, 015001.
15 N. C. Hogan, B. D. Hemond, D. M. Wendell, A. J. Taberner and I. W. Hunter, *Conf. Proc. IEEE Eng. Med. Biol. Soc.*, 2006, 5611–5616.
16 Y. Tagawa, N. Oudalov, C. W. Visser, I. R. Peters, D. van der Meer, C. Sun, A. Prosperetti and D. Lohse, *Phys. Rev. X*, 2012, **2**, 031002.
17 N. C. Hogan, B. D. Hemond, D. M. Wendell, A. J. Taberner and I. W. Hunter, *Proceedings of the 28th IEEE EMBS Annual International Conference*, New York City, USA, 2006.
18 C. Weller and M. Linder, *JAMA*, 1966, **195**, 844–847.
19 D. L. Bremseth and F. Pass, *Diabetes Technology & Therapeutics*, 2001, **3**, 225–232.
20 B. G. Weniger, *in Innovative Administration Systems for Vaccines*, Rockville, Maryland, 2003.
21 E. L. Giudice and J. D. Campbell, *Advanced Drug Delivery Reviews*, 2006, **58**, 68–89.
22 M. A. F. Kendall, *Handbook of Experimental Pharmacology: Drug Delivery*, 2010, **197**, 193–219.
23 C. Sun, E. Can, R. Dijkink, D. Lohse and A. Prosperetti, *J. Fluid Mech.*, 2009, **632**, 5–16.
24 V. S. Thakoersing, G. S. Gooris, A. Mulder, M. Rietveld, A. El Ghalbzouri and J. A. Bouwstra, *Tissue Eng.*, 2012, **18.**
25 V. S. Thakoersing, M. O. Danso, A. Mulder, G. Gooris, A. El Ghalbzouri and J. A. Bouwstra, *Exp. Dermatol.*, 2012, **21**, 865–870.
26 A. El Ghalbzouri, R. Siamari, R. Willemze and M. Ponec, *Toxicology in Vitro*, 2008, **97**, 1311–1320.